National Aeronautics and Space Administration

NASA LaRC and ARC

Material Response Modeling

Jeremie Meurisse
Eric Stern

July 12th, 2021

EDL Summer Seminar Series

Material Response Modeling Outline

- Introduction
- Material response model
  - Pure conduction
  - Porous media
    - Governing equations
    - Material properties
    - Pyrolysis gas modeling
    - Surface recession
    - Surface balance
- Material response codes
- Simulations results
- Summary

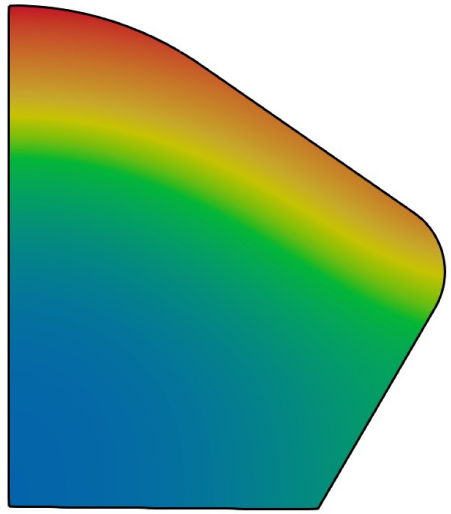

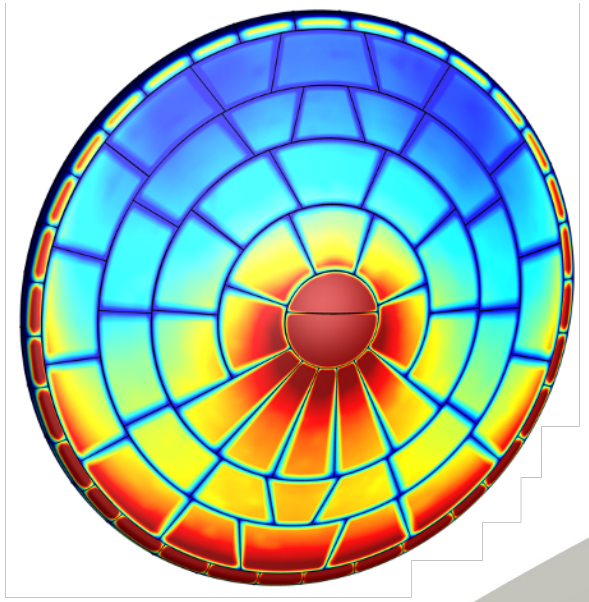

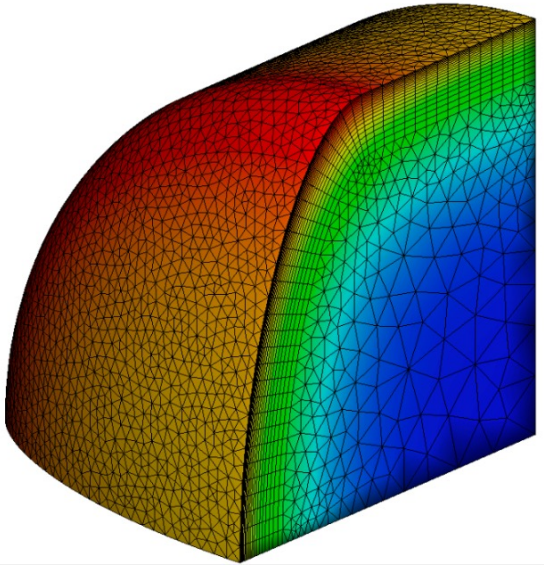

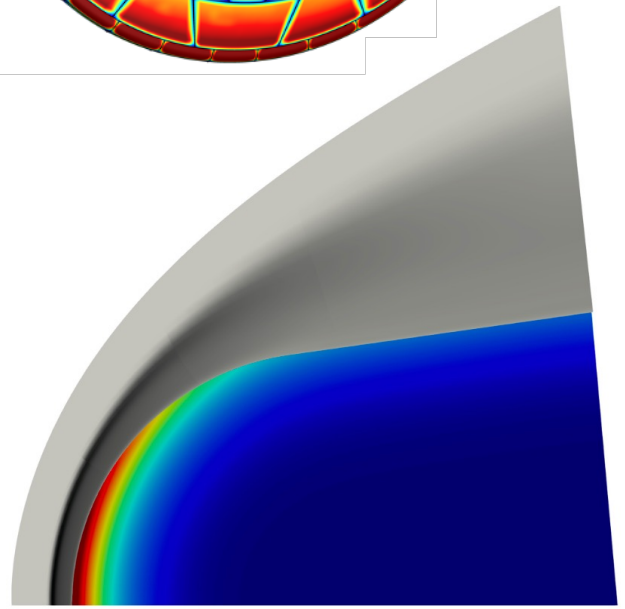

Our Main Goal: Predictive Material Response Modeling

Predictive modeling based on previous mission flight data

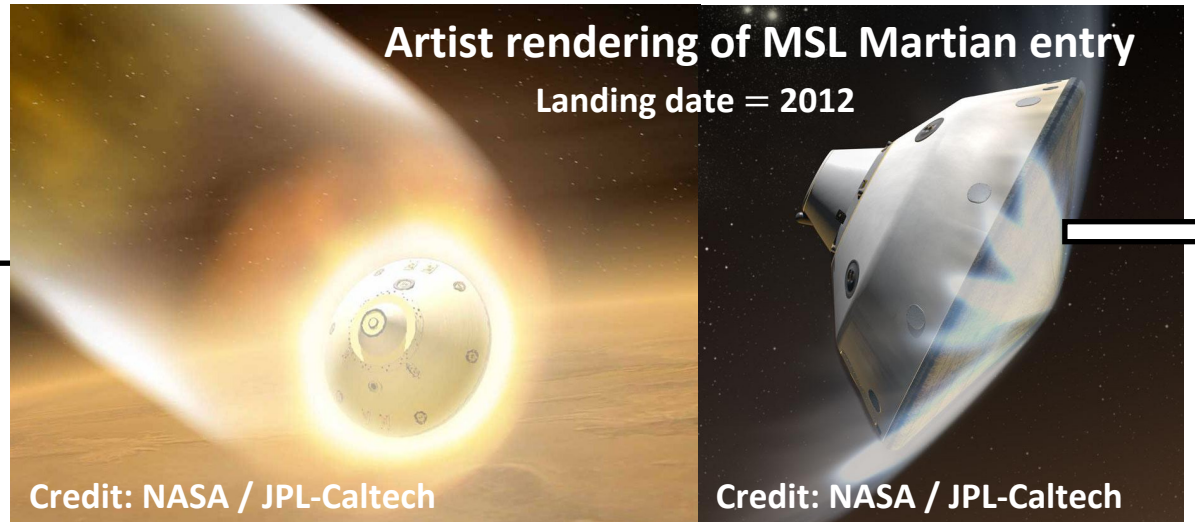

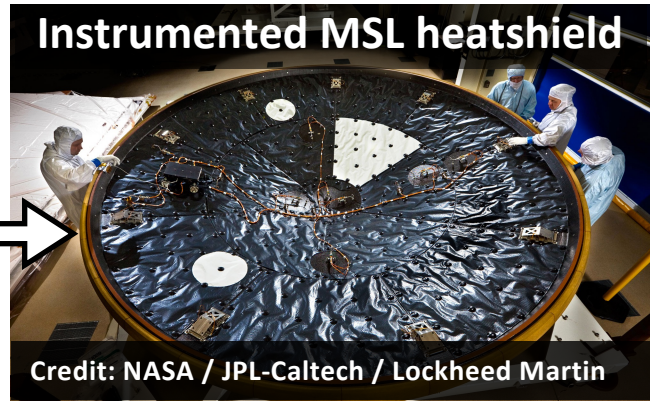

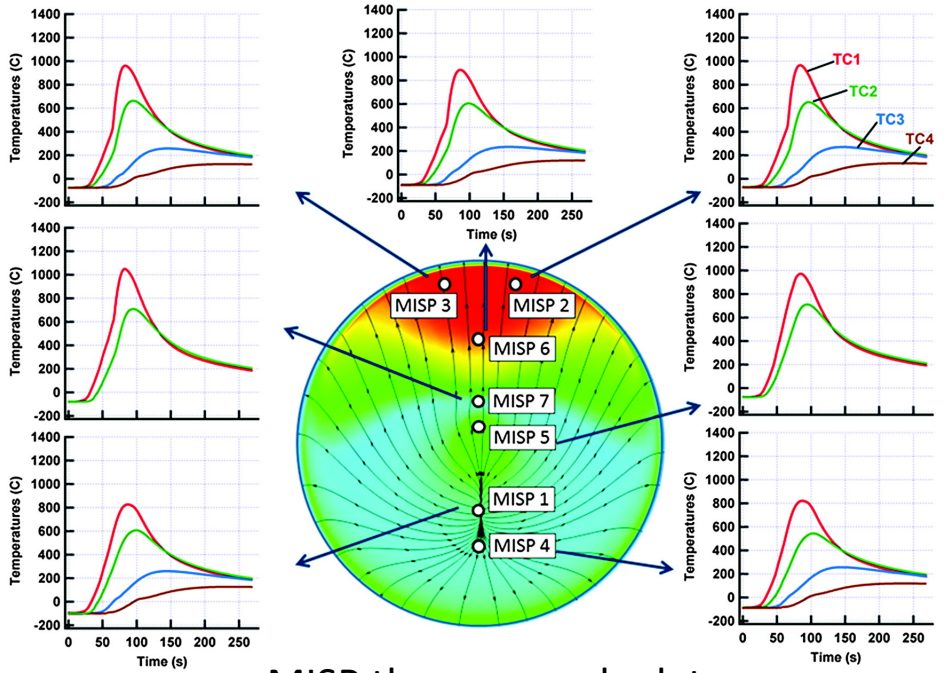

MISP thermocouple data obtained during MSL entry [1].

TPS materials for NASA missions

Stack of TPS and substructure for the MSL heatshield

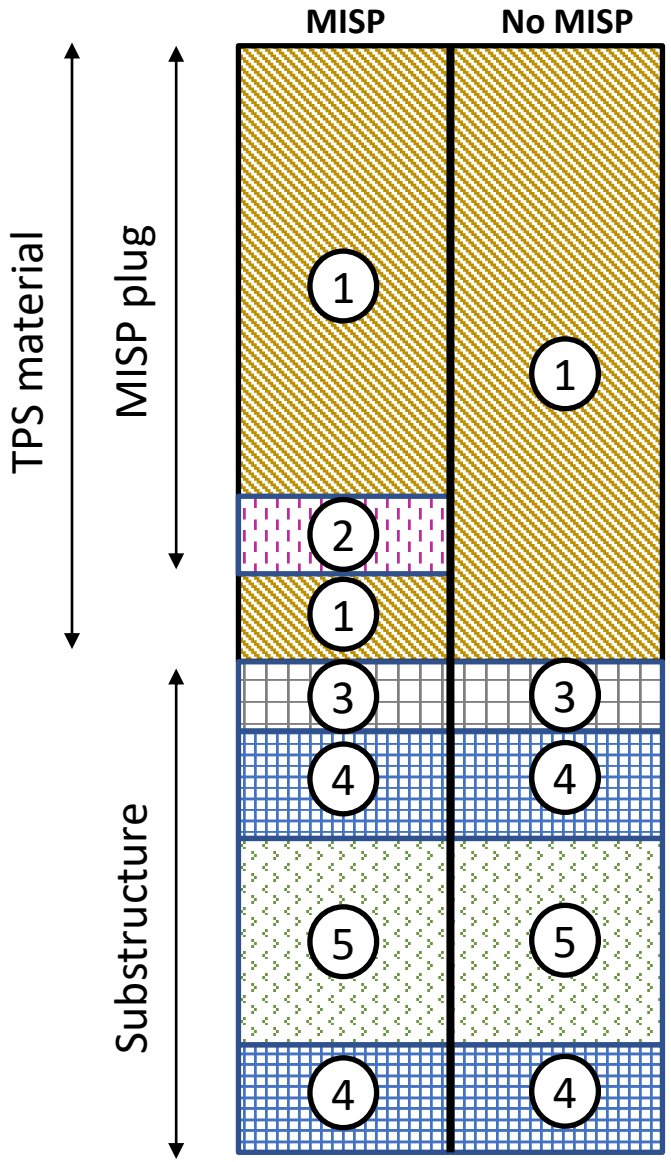

#	Material	Material Response Type	Thickness [mm]		
			Nose	Flank	Outer Flank
1	PICA	Flow in porous media	28.96 & 2.54		
2	RTV bonding agent	Flow in porous media	0.25		
3	Epoxy adhesive	Pure conduction in a solid	0.30		
4	Carbon facesheets	Pure conduction in a solid	0.51	1.02	2.54
5	Aluminum honeycomb	Pure conduction in a solid	63.5		

This table details the material stack for the MSL heatshield in 3 different zones: Nose, Flank and Outer Flank. While the PICA thickness was uniform (31.75 mm), the substructure stack varied depending on the location. The outer flank have considerably thicker carbon facesheets and a denser aluminum honeycomb [1].

Pure conduction in a solid - Energy equation

$$c_{p,s}\rho_s\partial_t T = \partial_{\mathbf{x}}\cdot\left(\underline{\underline{\mathbf{k_s}}}\cdot\partial_{\mathbf{x}}T\right)$$

$c_{p,s}$ = Solid heat capacity [J/kg/K]

ρ_s = Solid density [kg/m^3]

$\underline{\underline{\mathbf{k_s}}}$ = Solid thermal conductivity [W/m/K]

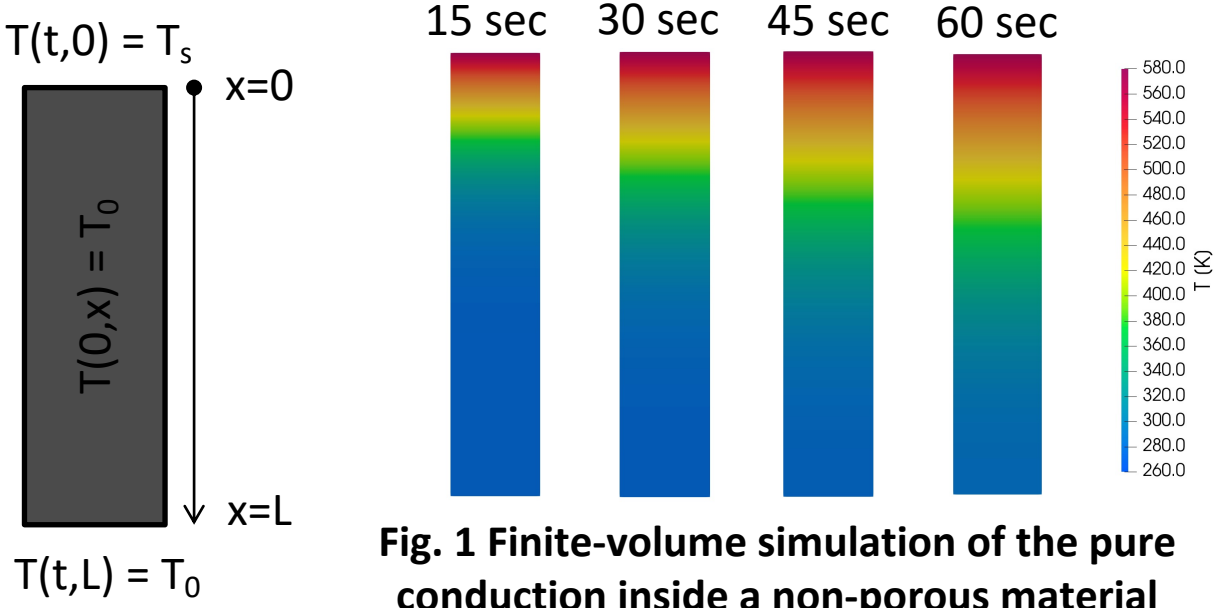

Fig. 1 Finite-volume simulation of the pure conduction inside a non-porous material

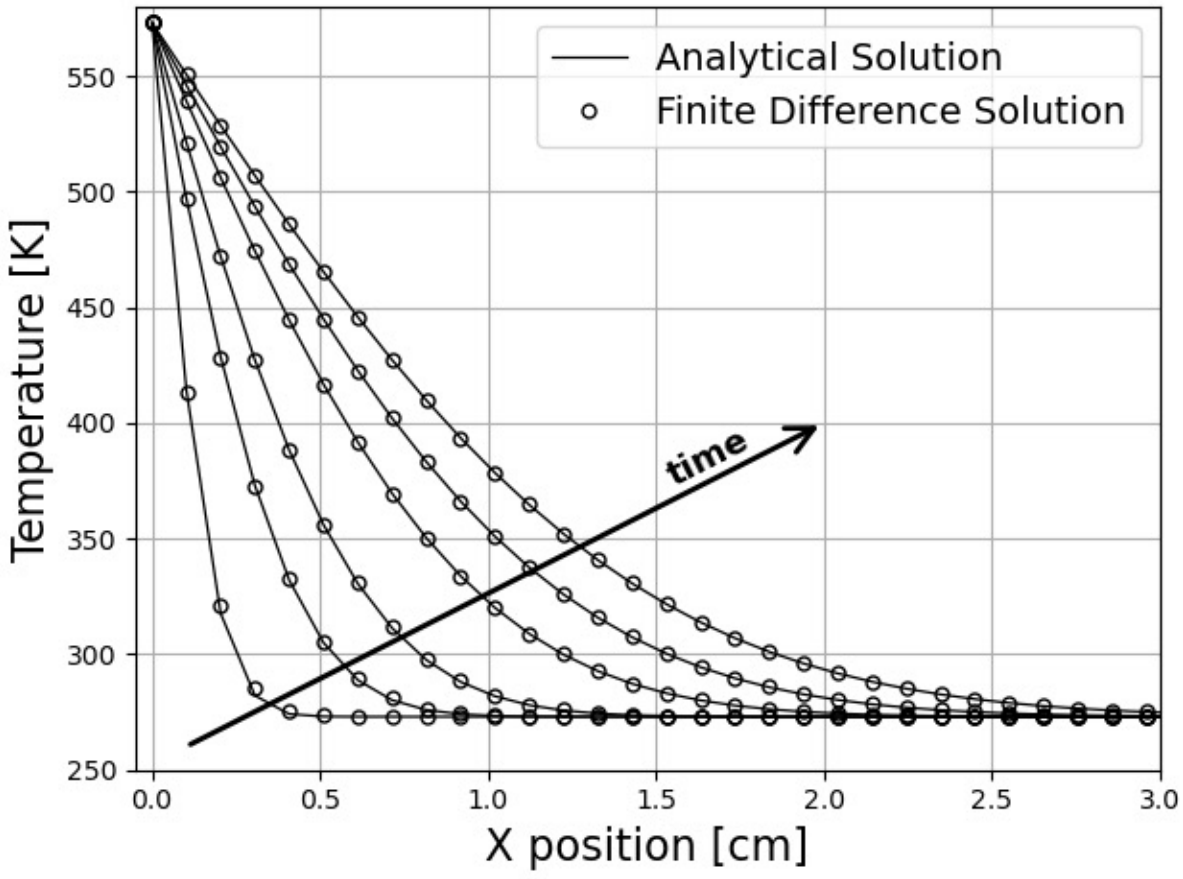

Fig. 2 Computation of the pure conduction inside a non-porous material compared to analytical solution.

Source code available here: https://tinyurl.com/ymdz8ddf

Porous TPS materials for NASA missions

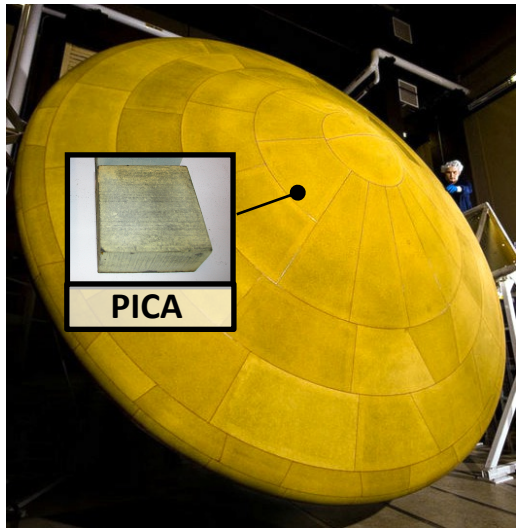

Fig.1 MSL heatshield was made of PICA [2].

Fig. 2 PICA at the micro-scale from Pr. Panerai (UIUC).

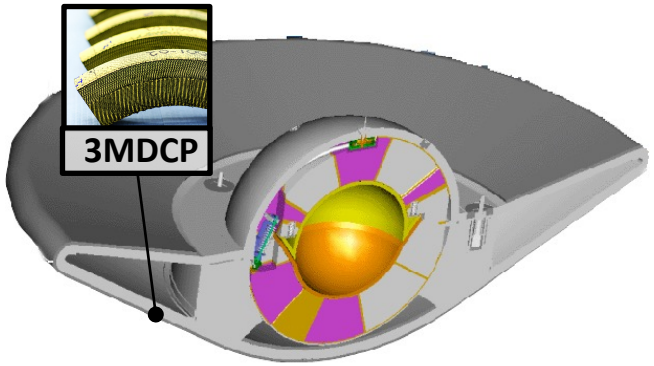

Fig.3 MSR-EEV heatshield might be made of 3MDCP [3].

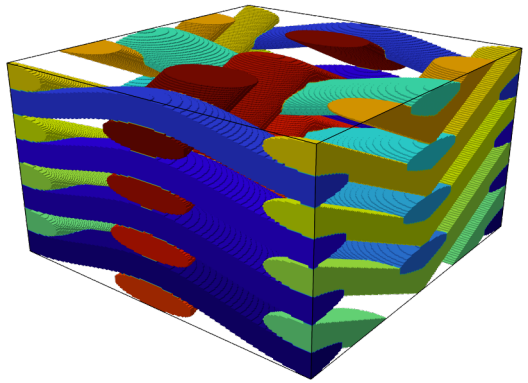

Fig. 4 3MDCP at the micro-scale from Semeraro (TSM).

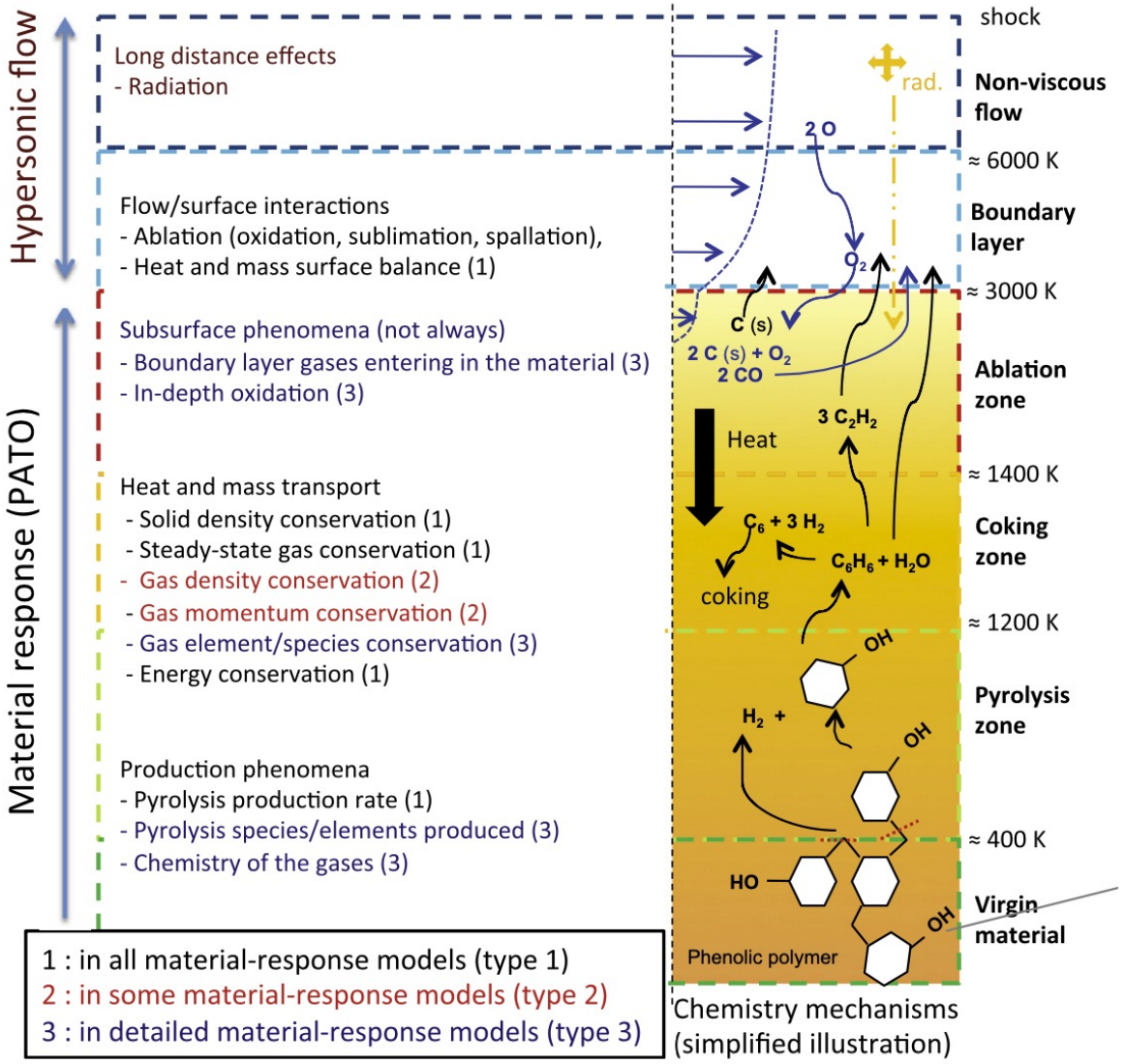

Fig. 5 Phenomenology of porous carbon/phenolic ablative materials [4].

Material Response Model - Mass conservation

Flow in porous media

$$\partial_t(\epsilon_g \rho_g) + \partial_{\mathbf{x}} \cdot (\epsilon_g \rho_g \mathbf{v}_g) = \Pi$$ Mass conservation

$$\rho_g = \frac{p_g M_g}{RT}$$ Ideal gas law

$$\mathbf{v}_g = -\frac{\perp}{\epsilon_g \mu_g} \underline{\underline{\mathbf{K_s}}} \cdot \partial_{\mathbf{x}} p_g$$ Darcy's law

The gaseous pressure is computed implicitly using

$$\partial_t(\beta_g p_g) - \partial_{\mathbf{x}} \cdot \left(\underline{\underline{\gamma_g}} \cdot \partial_{\mathbf{x}} p_g \right) = \Pi$$

$$\beta_g = \frac{\epsilon_g M_g}{RT}$$

$$\underline{\underline{\gamma_g}} = \frac{p_g M_g}{\mu_g RT} \underline{\underline{\mathbf{K}_s}}$$

Experiments

Computed

- ϵ_g = Gaseous volume fraction [-]
- ρ_g = Gaseous density [kg/m^3]
- $\mathbf{v}_g$ = Gaseous velocity [m/s]
- Π = Total pyrolysis gas production [kg/m^3/s]
- p_g = Gaseous pressure [Pa]
- M_g = Molar mass [kg/mol]
- R = Universal gas constant [J/kg/mol]
- T = Temperature [K]
- μ_g = Gaseous viscosity [kg/m/s]
- $\underline{\underline{\mathbf{K_s}}}$ = Solid permeability [m^2]

Material Response Model – Energy conservation

Flow in porous media

Energy conservation

$$\partial_t(\rho_t e_t) + \partial_{\mathbf{x}}\cdot(\epsilon_g \rho_g h_g \mathbf{v}_g) = \partial_{\mathbf{x}}\cdot\ (\underline{\underline{\mathbf{k_s}}} \cdot \partial_{\mathbf{x}} T)$$

Total storage energy

$$\rho_t e_t = \epsilon_g \rho_g e_g + \sum_{i\in[1,N_p]} (\epsilon_i \rho_i h_i)$$

The temperature is computed implicitly using

$$\sum_{i\in[1,N_p]} [(\epsilon_i \rho_i c_{p,i})\partial_t T + h_i \partial_t(\epsilon_i \rho_i)] =$$

$$\partial_{\mathbf{x}}\cdot\ (\underline{\underline{\mathbf{k_s}}} \cdot \partial_{\mathbf{x}} T) - \partial_t(\epsilon_g \rho_g h_g - \epsilon_g p_g)$$

$$- \partial_{\mathbf{x}}\cdot(\epsilon_g \rho_g h_g \mathbf{v}_g)$$

T = Temperature [K]

N_p = Number of solid phases

ϵ_i = Volume fraction of solid phase i [-]

ρ_i = Density of solid phase i [kg/m^3]

$c_{p,i}$ = Heat capacity of solid phase i [J/kg/K]

h_i = Enthalpy of solid phase i [J/kg]

h_g = Gaseous enthalpy [J/kg]

$\underline{\underline{\mathbf{k_s}}}$ = Solid thermal conductivity [W/m/K]

Experiments

Computed

Material Response Model – Material properties

Instruments	Material properties characterization
Thermal Gravimetric Analysis (TGA)	Measures the mass loss of a TPS material in wide range of temperatures and studies the char yield.
Differential Scanning Calorimetry (DSC)	Measures the glass transition temperature and specific heat capacity of TPS materials.
Laser Flash Analysis (LFA)	Measures the thermal diffusivity of TPS materials (for thermal conductivity determination).
Dilatometer	Measures the thermal expansion of TPS materials.
Scanning Electron Microscopy (SEM)	Characterizes the morphology of TPS materials (for recession measurements).

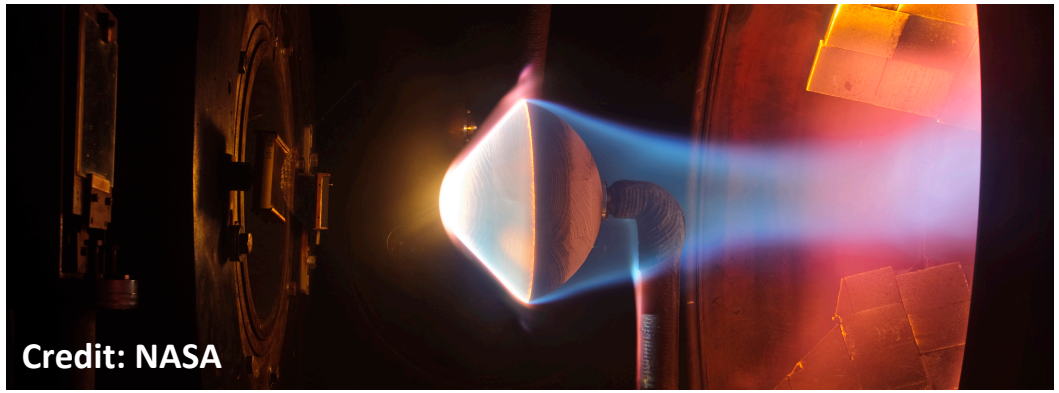

Fig. 1 The NASA arc-jet facilities provide essential experimental data on TPS materials.

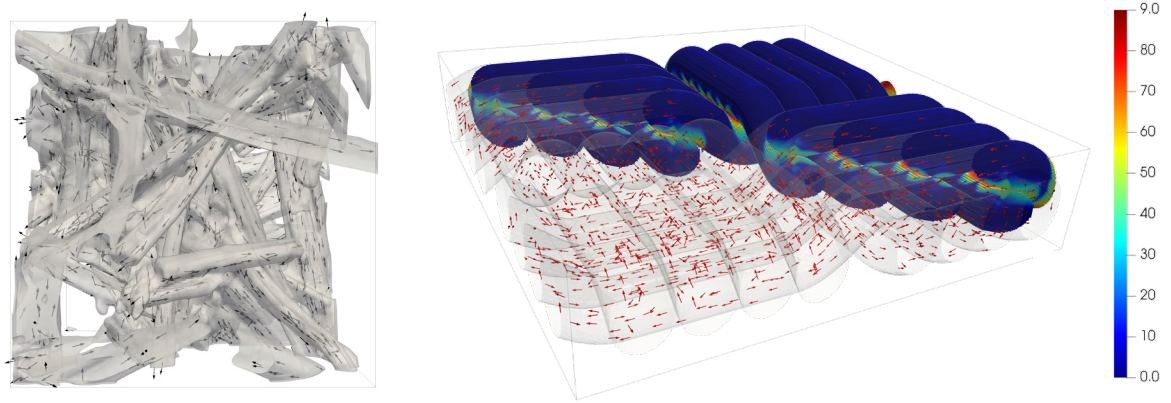

Fig. 3 Fiber and weave orientation from F. Semeraro (TSM).

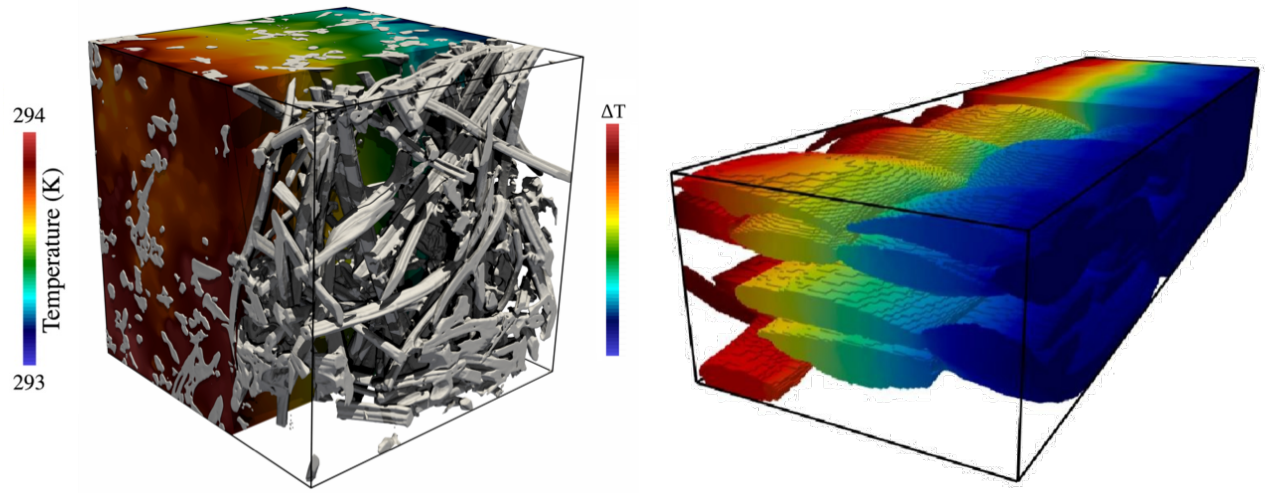

(a) Fibrous material. (b) Woven material.

Fig. 4 Effective thermal conductivity from F. Semeraro (TSM).

Material Response Model – Permeability

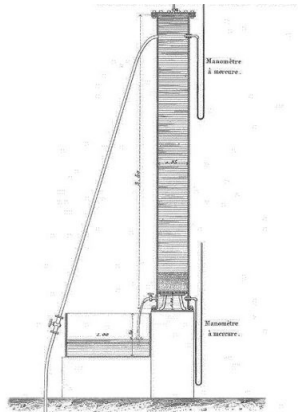

Fig. 1 Henry Darcy's experiments from 1856 [5].

Darcy's law describes the flow of a fluid through a porous medium [7].

$$\mathbf{v}_\mathrm{g} = -\frac{1}{\epsilon_\mathrm{g}\mu_\mathrm{g}}\underline{\underline{\mathbf{K_s}}} \cdot \partial_\mathbf{x} p_\mathrm{g}$$

Effective permeability is computed at the micro-scale by solving the equation of motion for Stokes flow

$$-\mu_\mathrm{g}\partial_\mathbf{x}^2\mathbf{v}_\mathrm{g} + \partial_\mathbf{x} p_\mathrm{g} = \mathbf{f}$$

The Klinkenberg correction $\underline{\underline{\beta}}$ can be added to the effective solid permeability tensor in order to account for slip effects at the pore scale when the Knudsen number is large (rarefied regime) [6,8].

$$\mathbf{v}_\mathrm{g} = -\frac{1}{\epsilon_\mathrm{g}}\left(\frac{1}{\mu_\mathrm{g}}\underline{\underline{\mathbf{K_s}}} + \frac{1}{p_\mathrm{g}}\underline{\underline{\beta}}\right) \cdot \partial_\mathbf{x} p_\mathrm{g}$$

$$\underline{\underline{\beta}} = \text{Klinkenberg correction } [\mathrm{m}^2/\mathrm{s}]$$

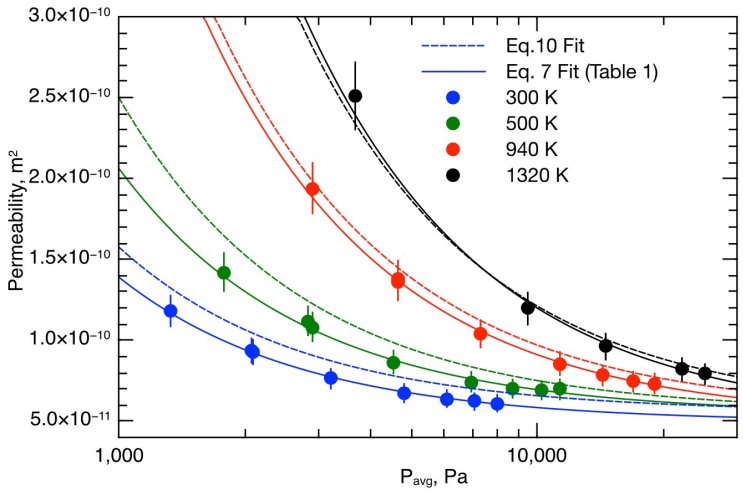

Fig. 2 Permeability experiments for FiberForm using a flow-tube [6].

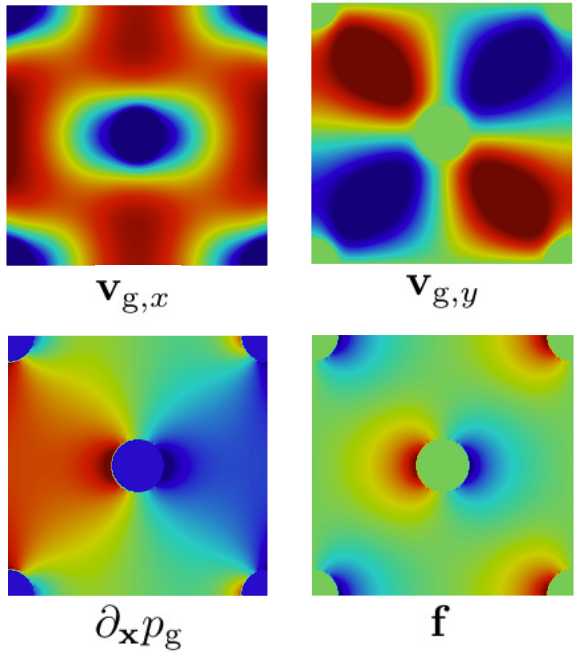

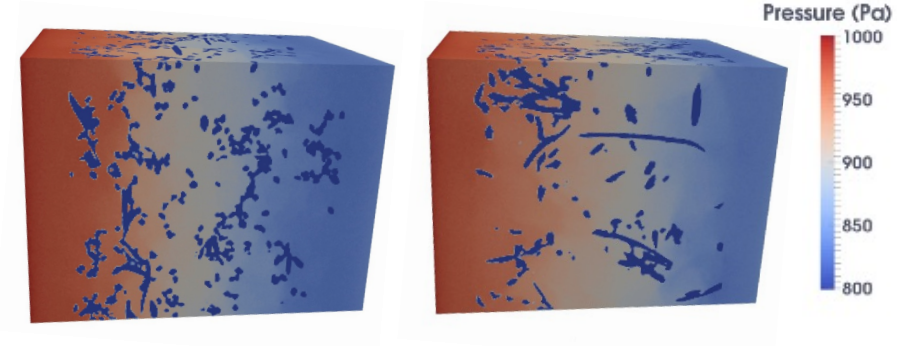

Fig. 3 Pressure for the flow of argon through FiberForm using DSMC [8].

Material Response Model - Pyrolysis

$$\partial_t(\chi_{i,j}) = (1-\chi_{i,j})^{m_{i,j}}\ T^{n_{i,j}}\mathcal{A}_{i,j}\exp\left(-\mathcal{E}_{i,j}/\mathcal{R}T\right)$$

$$i \in N_s, \quad j \in P_i$$

$$\Pi = \sum_{k\in[1,N_e]}\sum_{i\in[1,N_p]}\sum_{j\in[1,P_i]} \zeta_{i,j,k}\,\epsilon_{i,0}\,\rho_{i,0}\,F_{i,j}\,\partial_t\chi_{i,j}$$

$\chi_{i,j}$ = Advancement of pyrolysis [-]

$\mathcal{A}_{i,j}$ = Arrhenius law pre-exponential coefficient [SI]

$\mathcal{E}_{i,j}$ = Arrhenius law activation energy [J/mol]

P_i = Number of subphases in solid phase i

$\zeta_{i,j,k}$ =Mass stoichiometric coefficient [-]

$F_{i,j}$ = Fraction of subphase j in phase i [-]

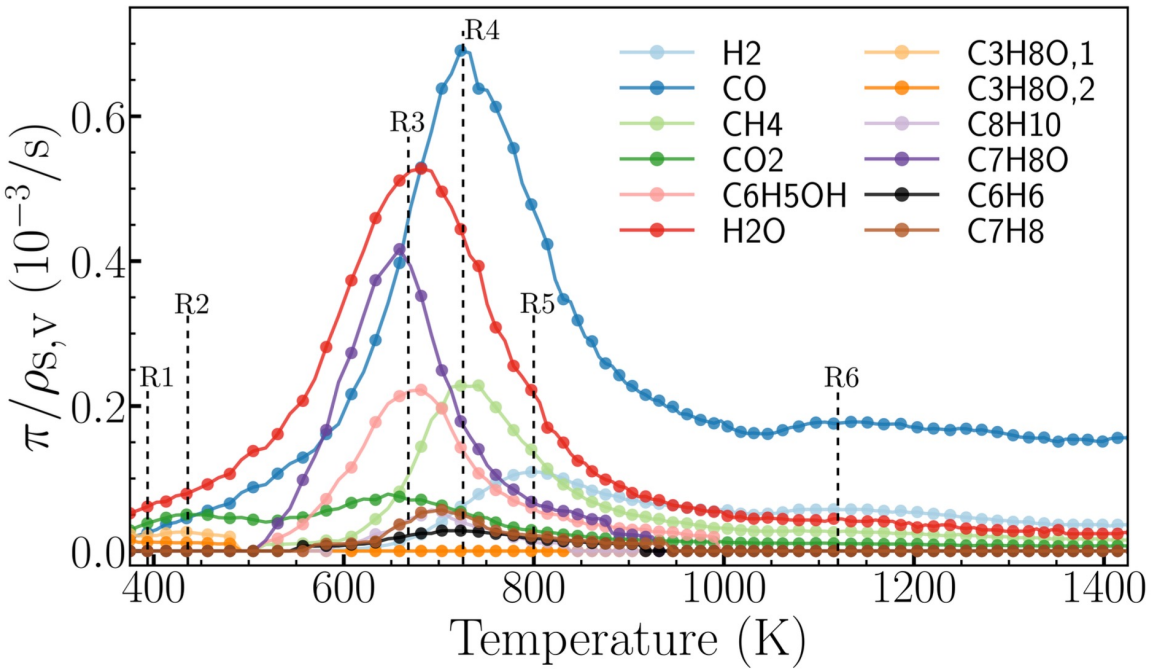

Fig. 1 Experimental measurements of the pyrolysis production rates for PICA [9].

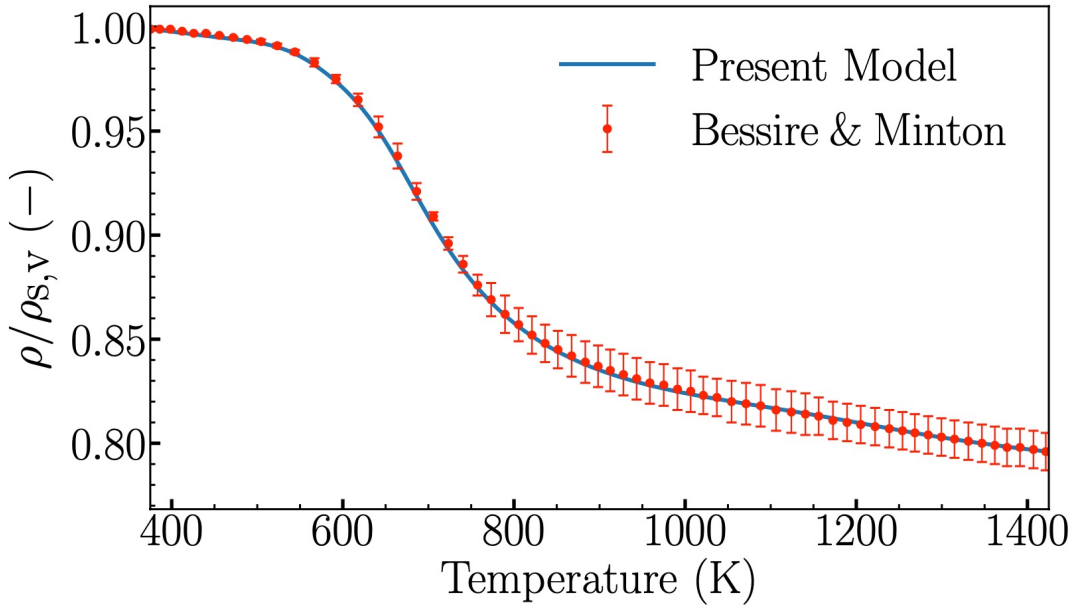

Fig. 2 Comparison between the pyrolysis model and the experimental TGA curve [10].

Material Response Model – Surface Recession [11]

Melting: solid → liquid

- Melting is a common ablation mechanism but doesn't absorb much energy.
- Rapid melt runoff due to aerodynamic shear results in significant but inefficient ablation.
- In contrast, a stable liquid layer on the surface can be attractive (due to the potential for vaporization).

Species	T_{melt} [K]	Heat of Fusion [J/g]
Al	933	397
Fe	1809	247
SiO_2	1996	150
TiO_2	2130	838
Al_2O_3	2315	1159

Vaporization: liquid → gas

- Vaporization absorbs significant amount of energy.
- Typically, liquid layers have low-moderate hemispherical emissivity (re-radiation ↘)
- Example with silica:

$$\mathrm{SiO_2(l)} \rightarrow \mathrm{SiO(g)} + {}^{1}/_{2}\ \mathrm{O_2(g)}$$

$$\Delta \mathrm{H_v} \approx 12.5\ \mathrm{kJ/g}$$

Sublimation: solid → gas

- Carbon sublimation is a highly endothermic process.

$$C(\mathrm{s}) \rightarrow aC_1(g) + \cdots + nC_n(g)$$

$$\mathrm{C_3(g)}\colon\ \Delta \mathrm{H_{sub}} \approx 22.7\ \mathrm{kJ/g}$$

- Predictions exhibit some sensitivity to species thermochemical data.

Oxidation: solid + O_2(g) → gas

- Oxidation is an exothermic process.
- Example with carbon graphite:

$$2\mathrm{C(s)} + \mathrm{O_2(g)} \rightarrow 2\mathrm{CO(g)} \qquad \Delta \mathrm{H_{comb}} \approx -4.17\ \mathrm{MJ/g}$$

- Material response codes usually assume thermochemical equilibrium that overestimates the surface recession for the carbon ablation at low surface temperatures.
- Realistic estimates require consideration of reaction-rate limited oxidation processes.

Spallation: mechanical erosion

- Spallation refers to thermostructural failure of the material and ejection of solid char and particulates. More common in organic resin composites than homogeneous materials
- All organic resin composites have a spallation threshold that usually increases with increasing density.

Material Response Model – Surface Mass Balance

$$C_{\mathrm{M}}(z_{k,\mathrm{w}} - z_{k,\mathrm{e}}) + z_{k,\mathrm{w}}\,(\dot{m}_{\mathrm{ca}} + \dot{m}_{\mathrm{pg}}) =$$

$$\dot{m}_{\mathrm{pg}}\ z_{k,\mathrm{pg}} + \dot{m}_{\mathrm{ca}}\ z_{k,\mathrm{ca}}$$

$$h_{\mathrm{w}} = \sum_{i \in N_{\mathrm{g}}} y_{i,\mathrm{w}}^{\mathrm{eq}}\ h_i \qquad B'_{\mathrm{ca}} = \frac{\dot{m}_{\mathrm{ca}}}{C_{\mathrm{M}}} \qquad B'_{\mathrm{pg}} = \frac{\dot{m}_{\mathrm{pg}}}{C_{\mathrm{M}}}$$

$$B'_{\mathrm{ca}} = \frac{B'_{\mathrm{pg}}\,(z_{k,\mathrm{pg}} - z_{k,\mathrm{w}}) + z_{k,\mathrm{e}} - z_{k,\mathrm{w}}}{z_{k,\mathrm{w}} - z_{k,\mathrm{ca}}}$$

C_M = Mass transfer coefficient [kg/m^2/s]

z = Elemental mass fraction [-]

y = Species mass fraction [-]

$\dot{m}$ = Mass flux [kg/m^2/s]

B' = Dimensionless blowing rate [-]

h = Enthalpy [J/kg]

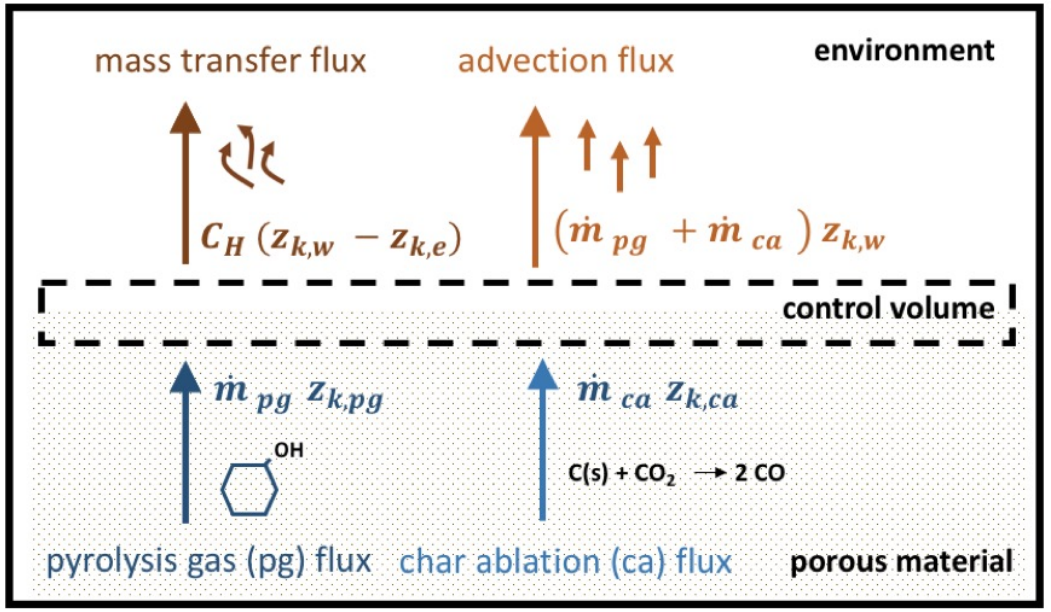

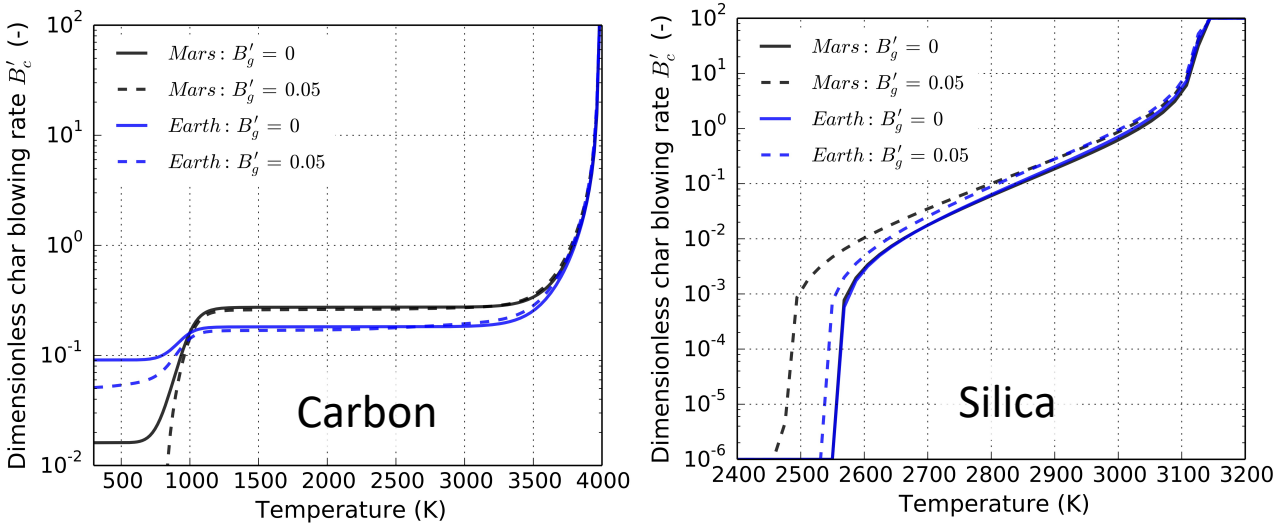

Fig. 1 Surface mass balance and B'_c profiles.

Material Response Model – Blowing correction

$$C'_H = C_H \frac{ln\left[1 + 2\lambda\left(B'_{pg} + B'_{ca}\right)\right]}{2\lambda\left(B'_{pg} + B'_{ca}\right)}$$

λ = Scaling factor [-]

C'_H = Corrected heat transfer coefficient [kg/m^2/s]

Environment	Scaling factor λ
Laminar	0.5
Turbulent	0.3

Table 1 Scaling factor for laminar and turbulent environments.

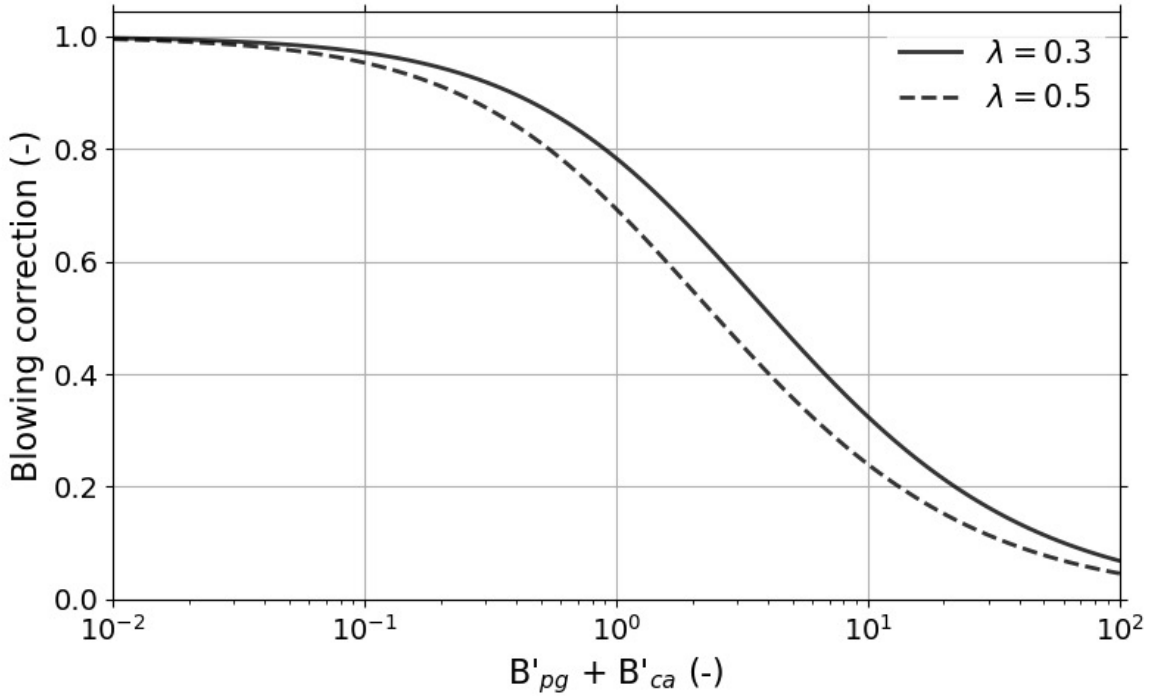

Fig. 1 Blowing correction in function of blowing rate.

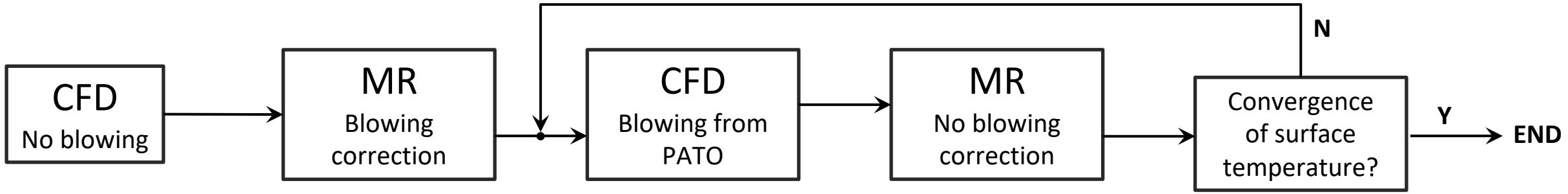

Fig. 2 Methodology of the two-way coupling (CFD↔MR) with pyrolysis blowing gases.

Material Response Model – Surface Energy Balance

$$\left[-\underline{\underline{\mathbf{k}}} \cdot \partial_x T\right] \cdot \mathbf{n} = q_{\mathrm{diff}} + \dot{m}_{\mathrm{ca}}(h_{\mathrm{ca}} - h_{\mathrm{w}}) + \dot{m}_{\mathrm{pg}}(h_{\mathrm{pg}} - h_{\mathrm{w}}) + q_{\mathrm{rad}}$$

$$q_{\mathrm{diff}} = C'_{\mathrm{H}}(h_{\mathrm{e}} - h_{\mathrm{w}})$$

$$q_{\mathrm{rad}} = \alpha_{\mathrm{w}} q_{\mathrm{pla}} - \varepsilon_{\mathrm{w}} \sigma \left(T^4 - T_{\infty}^4\right)$$

q = Heat flux [W/m^2]

α = Absorptivity [-]

ε = Emissivity [-]

σ = Stefan-Boltzmann constant [W/K^4/m^2]

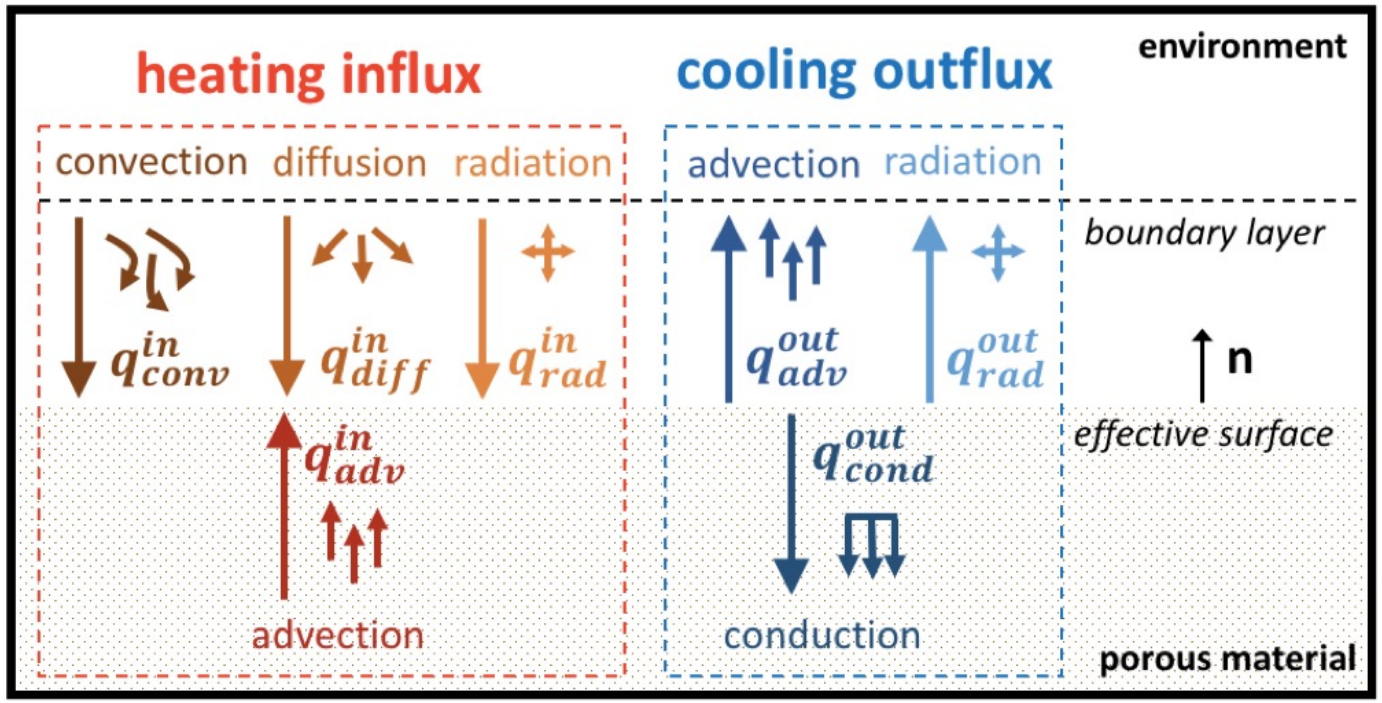

Fig. 1 Representation of the surface energy balance.

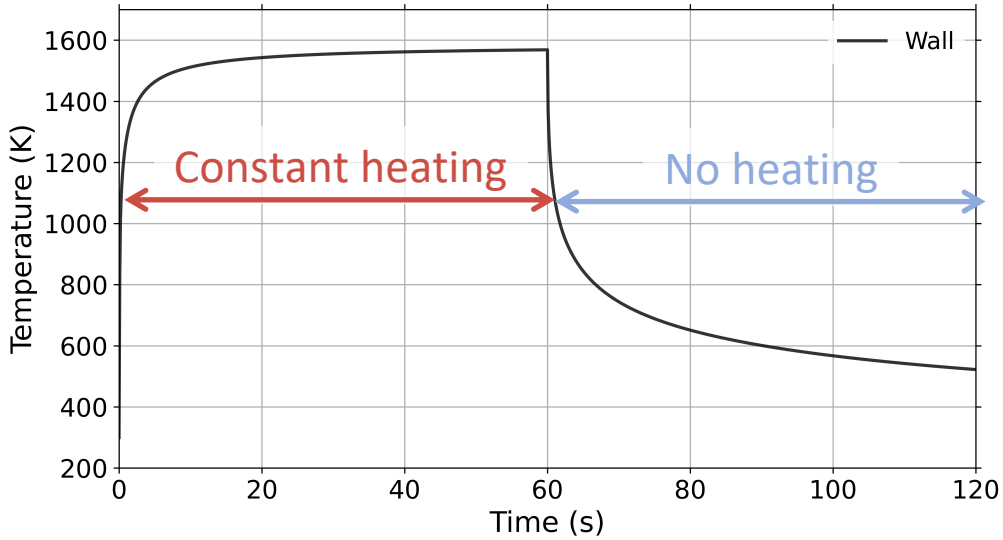

Fig.2 Surface temperature computed with constant heating.

Brief History of NASA Material Response Codes

CMA

- Charring Materials Ablation
- Moyer & Rindal (1968)
- Developed by Aerotherm
- Finite Difference
- Node-dropping scheme for ablation
- Still used today, believe it or not

FIAT

- **F**ully **I**mplicit **A**blation and **T**hermal response program
- Chen & Milos (1999)
- Implicit time stepping (more stable!)
- Grid compression for ablation
- Widely used across industry and NASA (MSL, Stardust, Mars2020, and many more)

TITAN

- Two-dimensional implementation of FIAT
- Chen & Milos (2001)
- Coupled with GASP/DPLR

3dFIAT

- Three-dimensional implementation of FIAT
- Chen & Milos (2005)

TITAN

- Two-dimensional implementation of FIAT
- Chen & Milos (2001)
- Coupled with GASP/DPLR

3dFIAT

- Three-dimensional implementation of FIAT
- Chen & Milos (2005)

PATO

- High-fidelity, multi-dimensional solver built on OpenFOAM
- Lachaud & Mansour (2014)
- Simple to implement and test new physical models

CHAR

- Multi-dimensional, finite-element (FEM) solver
- Amar et al. (2016)
- Primarily used for Orion

Icarus

- In-house finite volume, parallel, unstructured solver
- Schulz et al. (2017)
- US3D integration

2000's

2010's

Simulation results for the HyMETS arc-jet facility

CFD solutions using DPLR [12]

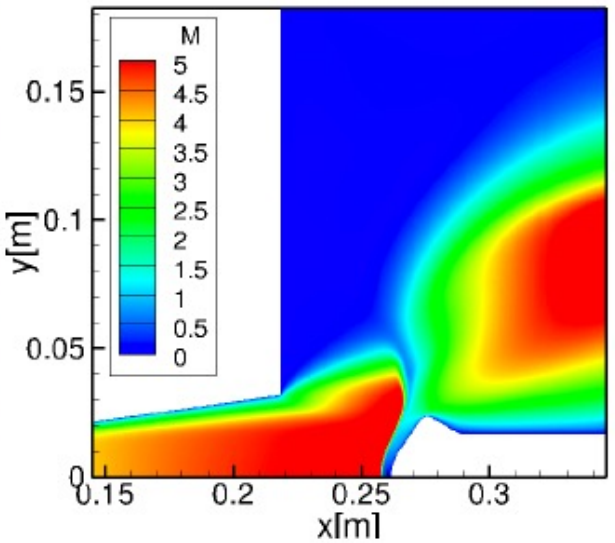

Fig. 1 Mach number contours.

The aerothermal environment of the HyMETS facility was simulated to provide the surface boundary conditions needed for the material response model. The flow field modeling includes chemical and thermal non-equilibrium state of the testing gas.

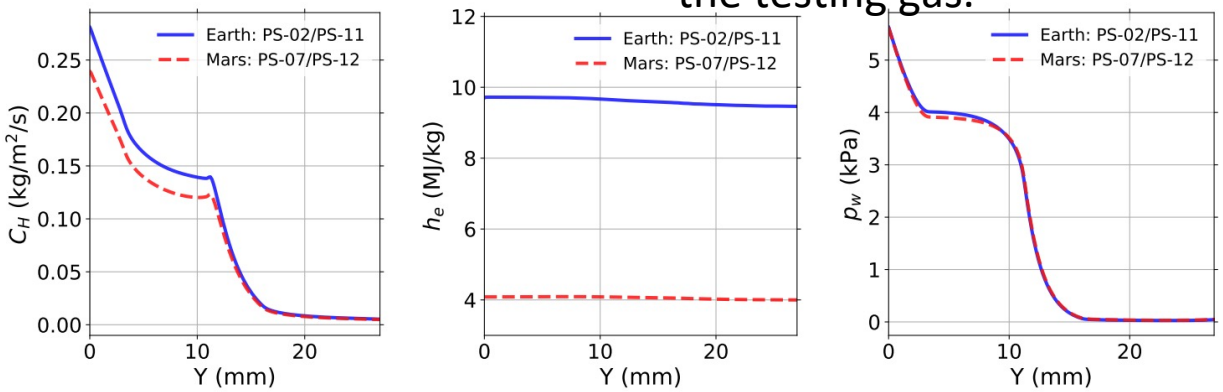

Fig. 2 Aerothermal environment at the sample surface.

Material response solutions using PATO [13]

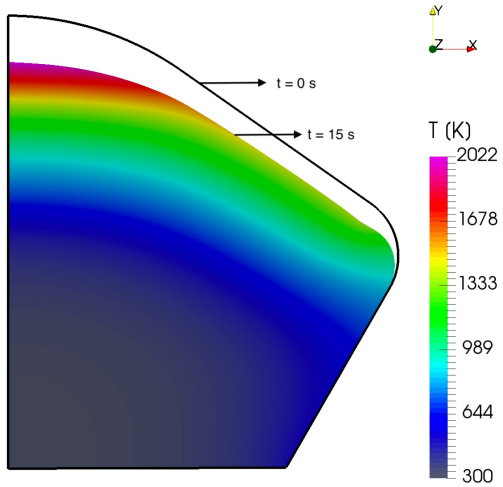

Fig. 3 Material response at 15 sec.

To reproduce the experiments, the sample was heated for 30 sec then cooled for 10 sec. The temperature measured by a pyrometer was compared to the simulated one and the in-depth temperatures were compared to the

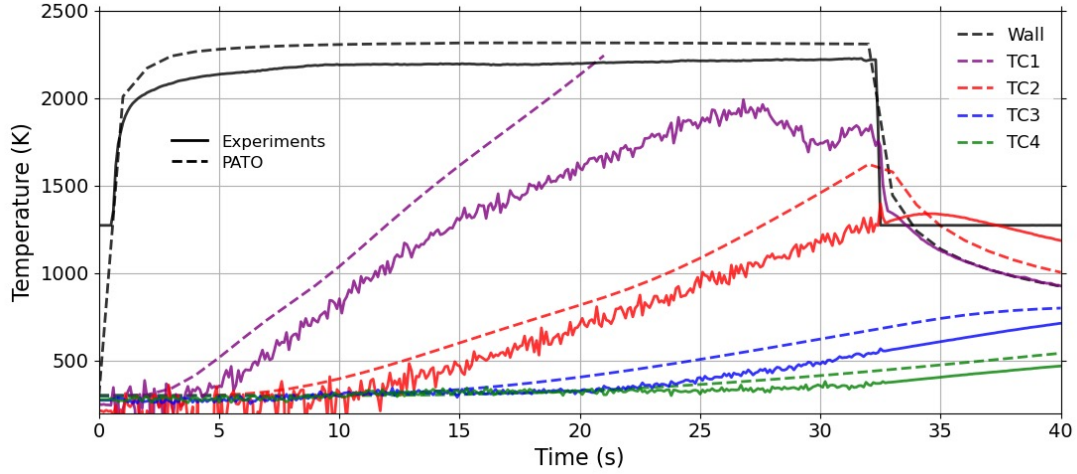

Fig. 4 Evolution in time of the material temperature.

Simulation results for the Mars Science Laboratory (MSL)

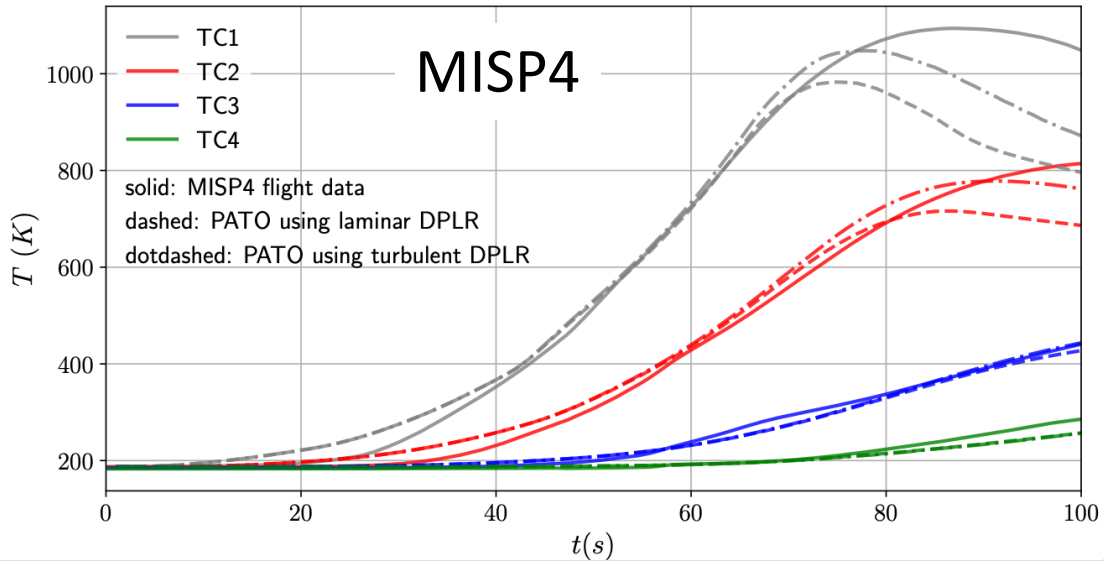

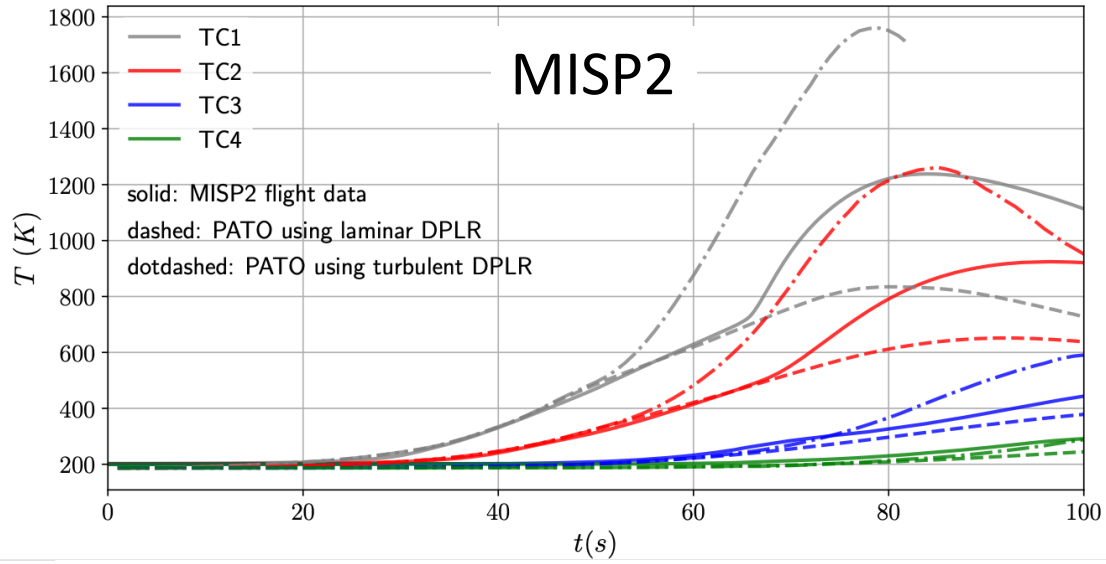

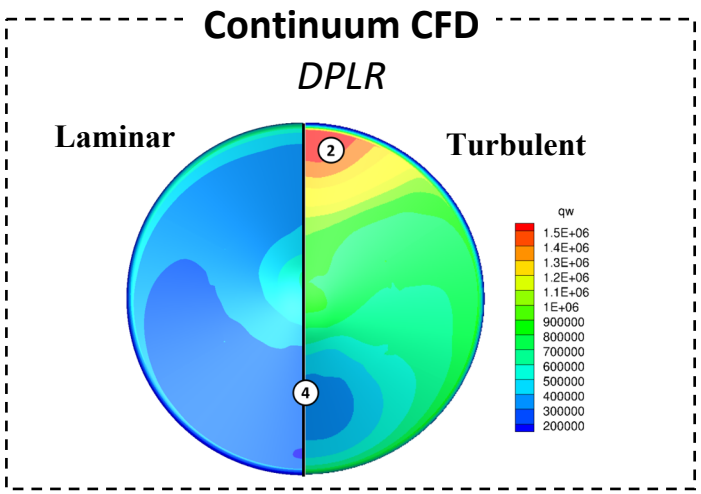

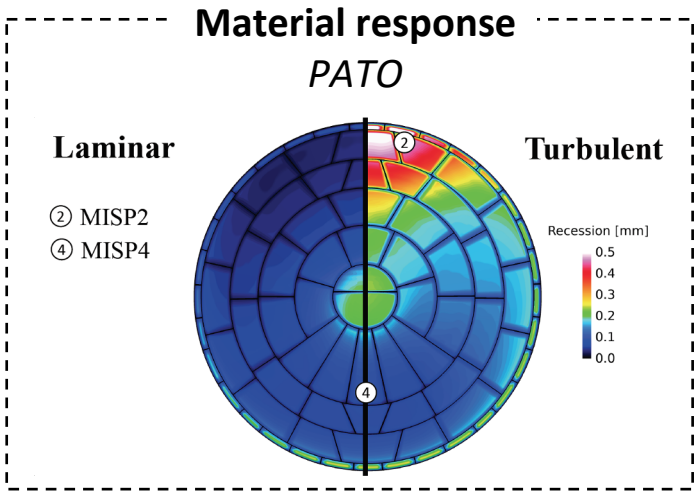

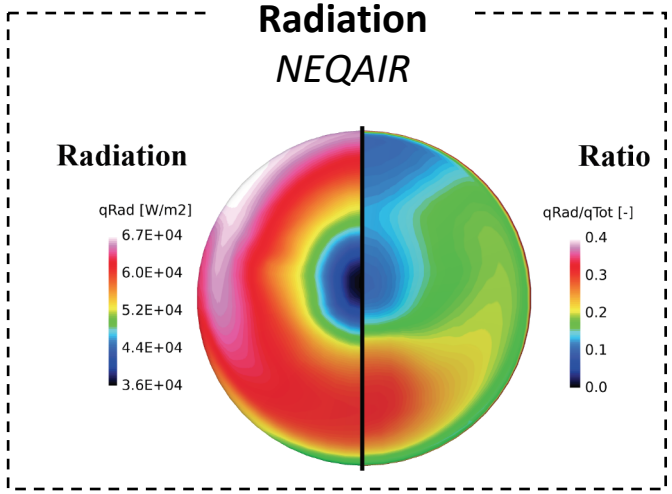

Fig. 1 Showing the MISP locations on the MSL heatshield and highlighting the codes used in this study. Comparison to the MISP flight data that provided in-depth temperature during the MSL entry [14].

Dragonfly Case Study: TPS Sizing

Objective: determine required PICA thickness such that bondline temperature limit is not exceeded

Trajectory
POST2

↓

Aerothermal Environment
DPLR/NEQAIR

↓

TPS Sizing
FIAT/Icarus

⇠ **Structure Defintion**
Lockheed

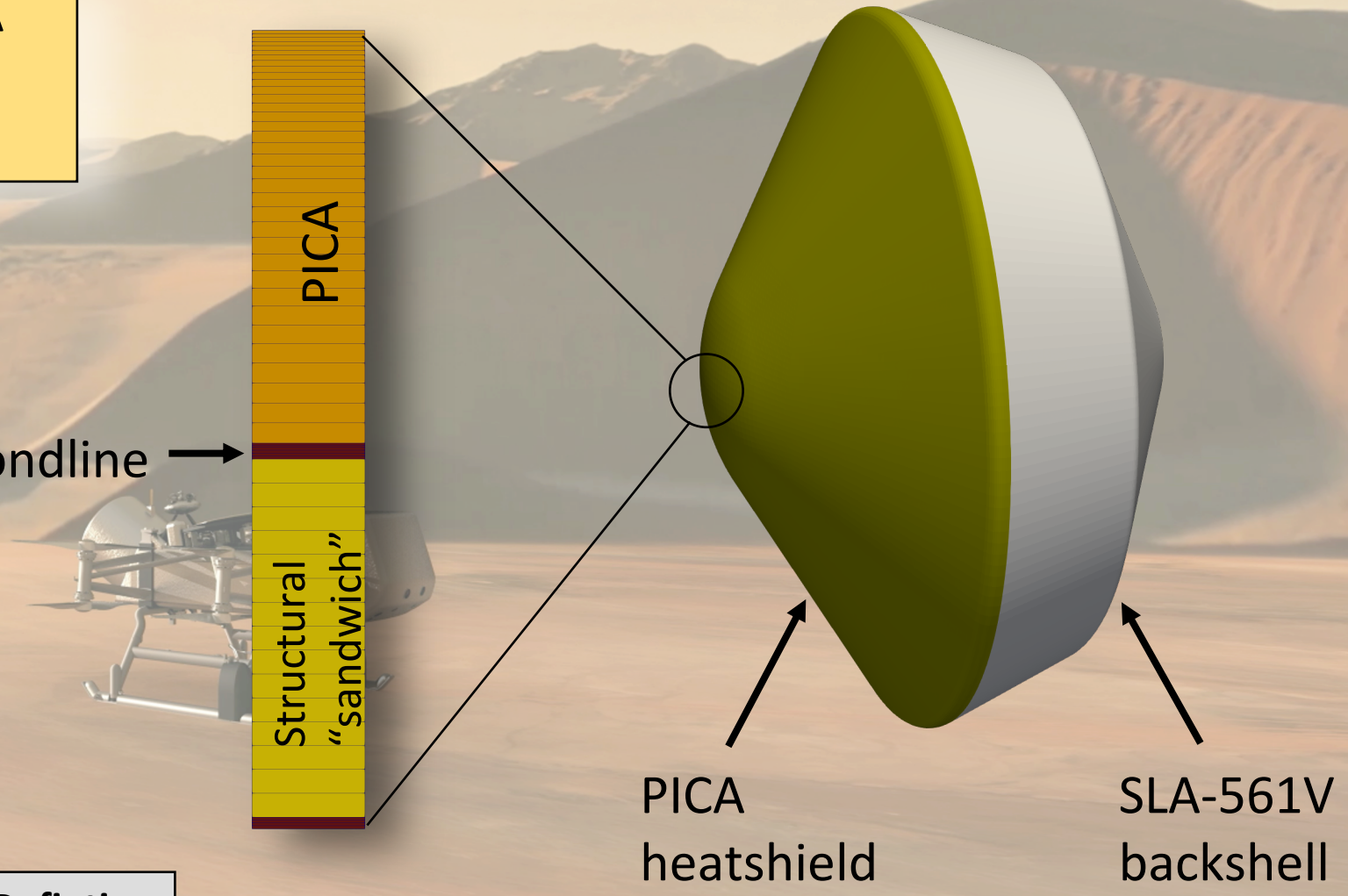

Dragonfly Case Study: TPS Sizing

Trajectory
POST2

Aerothermal Environment
DPLR/NEQAIR

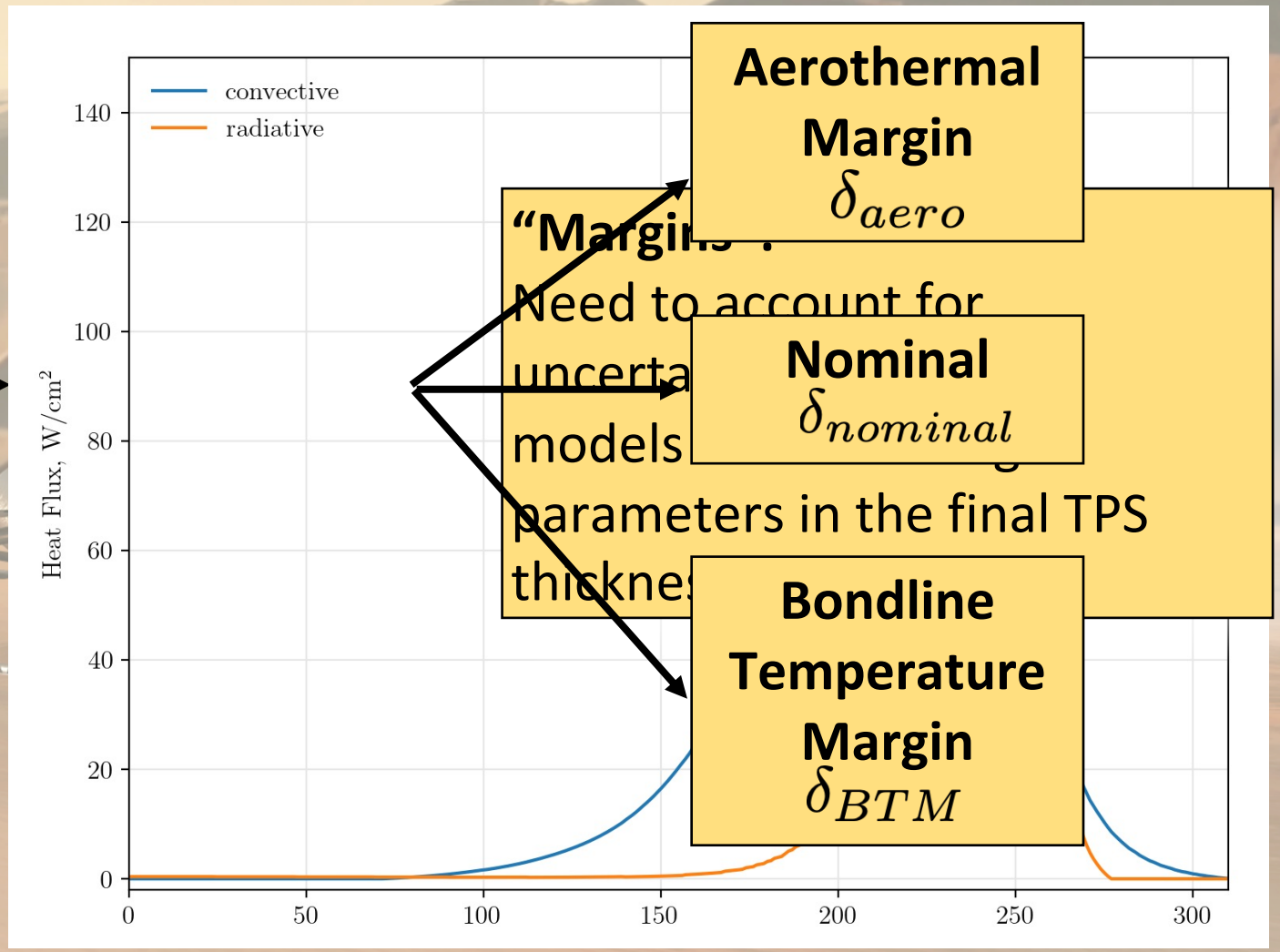

Aerothermal Margin
δ_{aero}

"Margins":
Need to account for uncerta… models … parameters in the final TPS thickne…

Nominal
$\delta_{nominal}$

Bondline Temperature Margin
δ_{BTM}

Dragonfly Case Study: TPS Sizing

Trajectory
POST2

Aerothermal Environment
DPLR/NEQAIR

Structure Defintion
Lockheed

TPS Sizing
FIAT/Icarus

Aerothermal Margin
δ_{aero}

Nominal
$\delta_{nominal}$

Bondline Temperature Margin
δ_{BTM}

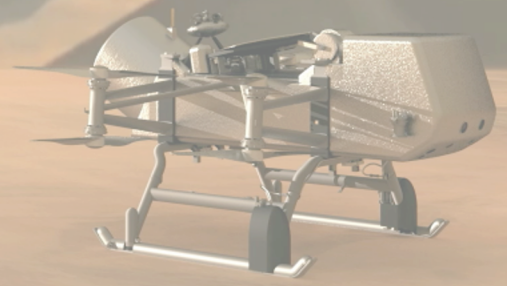

$$RSS = \delta_{nominal} + \sqrt{(\delta_{aero} - \delta_{nominal})^2 + (\delta_{BTL} - \delta_{nominal})^2}$$

Dragonfly Case Study: Convective Cooling

Titan entry is relatively benign from an aerothermal perspective, however…

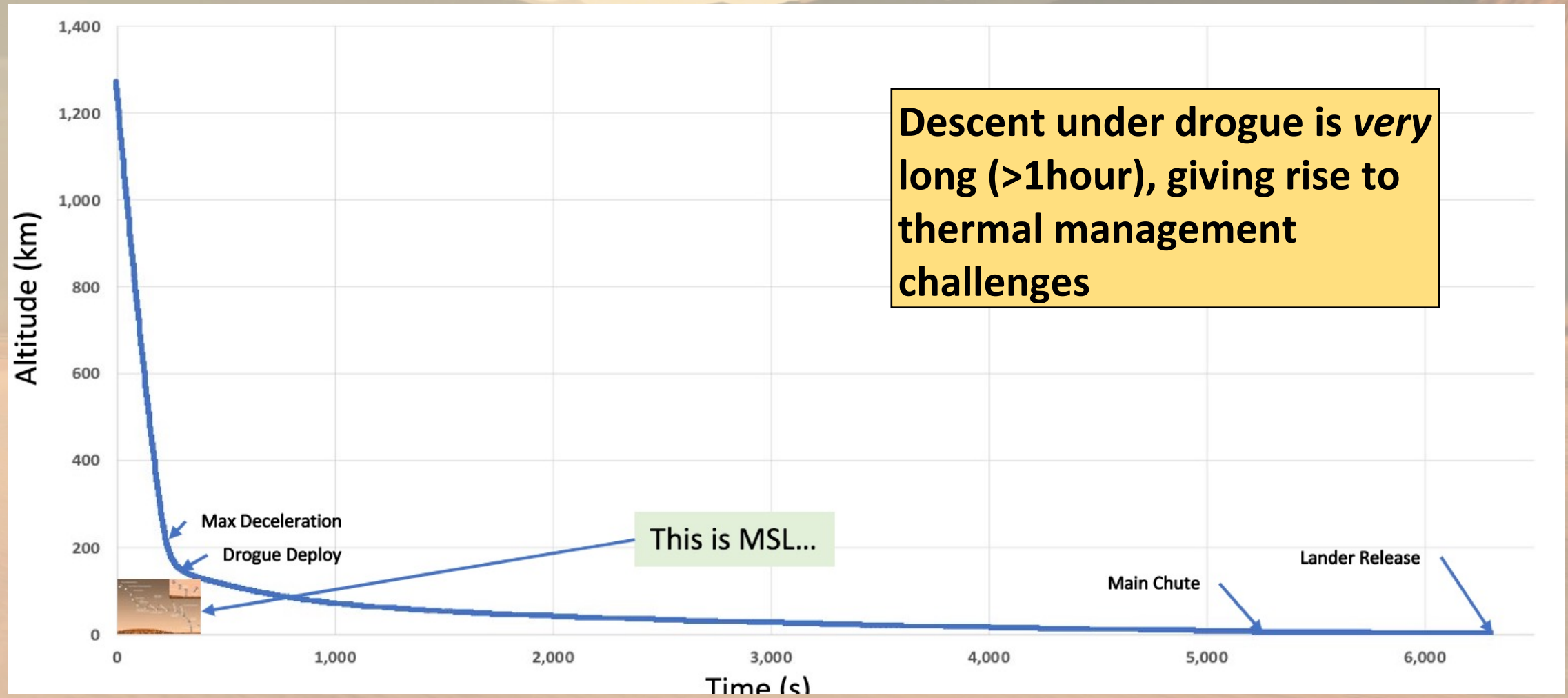

Descent under drogue is *very* long (>1hour), giving rise to thermal management challenges

Dragonfly Case Study: Convective Cooling

Objective: take advantage of cryogenic Titan atmosphere to cool aeroshell

Surface Energy Balance

$$q_{conv} + \alpha q_{rad} - \epsilon\sigma\left(T_w^4 - T_\infty^4\right) + C_T\left(T_\infty - T_w\right) - q_{cond} = 0$$

Convective Cooling Model

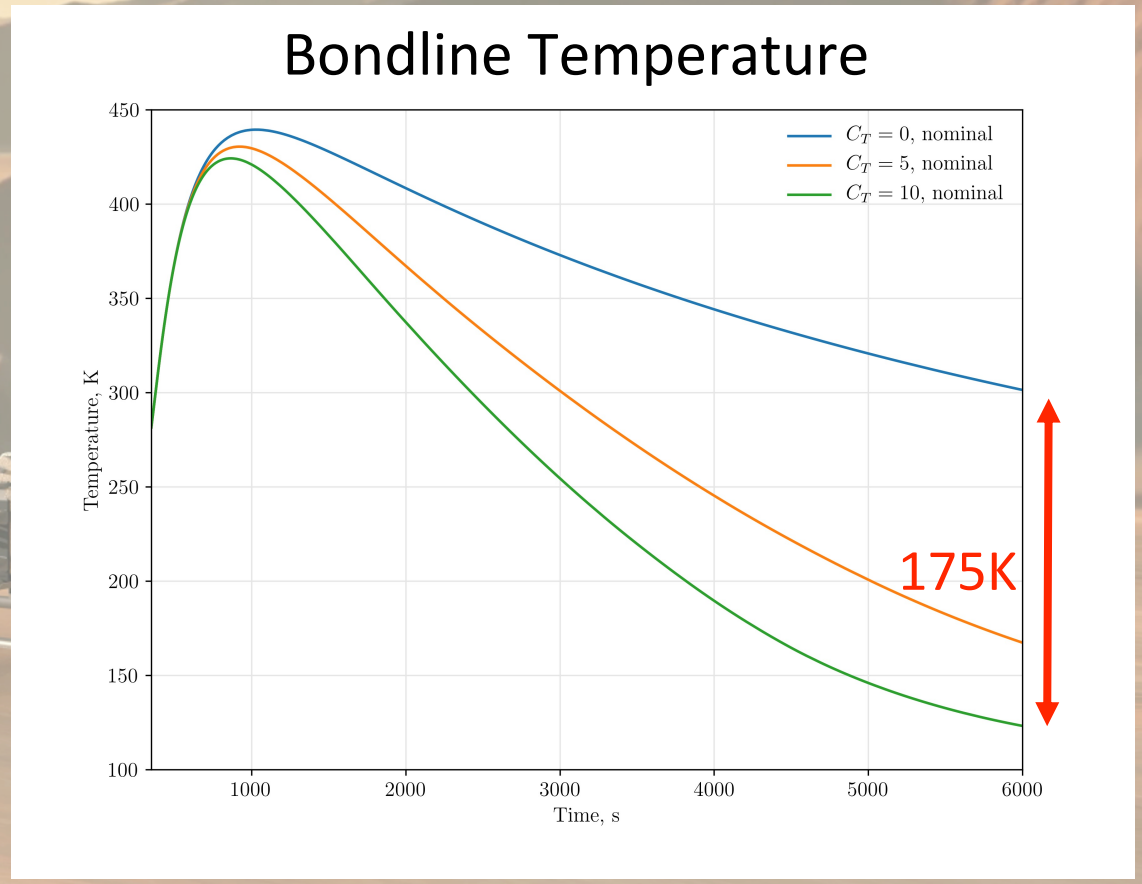

Material Response Modeling Summary

Conclusion

- The heatshield, made of a stack of materials (TPS + substructure), protects the space probe from the harsh environment during atmospheric entry.
- The non-porous materials can be modeled as pure conduction in a solid (energy equation).
- The porous materials can be modeled with more equations (mass/energy conservation and surface balance) including strong assumptions (e.g.: equilibrium) to simulate the complex physics in play.
- Teams at NASA have been developing material response codes since the 60s to help the design of future missions to Mars, Titan and beyond.
- Comparison of the material response simulations to experimental data from ground testing (e.g.: arc-jets) and flight data from previous missions (e.g.: MSL) considerably contributes to the development of predictive material models for future NASA missions.

Future work

- Modeling of Micro-Meteoroids and Orbital Debris (MMOD) impact on thermal protection materials.
- Including stress analysis in the material response models to account for mechanical erosion such as spallation and shear-induced mass removal.
- Improving material properties for TPS materials such as ADEPT, HEEET and PICA.
- Modeling of the fencing effect due to RTV between the tiles (MSL and Mars 2020 heatshield).
- Improving the model of transition from laminar to fully turbulent in the aerothermal environment.
- Adding the effect of a coating layer, such as NuSil, on top of the TPS material.
- Including more advanced coupling between the CFD and the material response.
- Implementing more detailed gas-surface interaction models such as finite-rate chemistry.

Material Response Modeling Summary

[1] T. White, et al. "Post-flight Analysis of Mars Science Laboratory's Entry Aerothermal Environment and Thermal Protection System Response." 44th AIAA Thermophysics Conference (2013).
[2] H. K. Tran, et al. "Phenolic impregnated carbon ablators pica as thermal protection system for discovery missions." NASA TM-110440, NASA, Washington, DC. (1997).
[3] R. Dillman, et al. "Development and Test Plans for the MSR EEV." 2nd International Planetary Probe Workshop (2004).
[4] J. Lachaud, et al. "A generic local thermal equilibrium model for porous reactive materials submitted to high temperatures." International Journal of Heat and Mass Transfer 108 (2017): 1406-1417.
[5] H. Darcy, "Les Fontaines Publiques de la Ville de Dijon.", Victor Dalmont, Paris (1856).
[6] F. Panerai, et al. "Experimental measurements of the permeability of fibrous carbon at high-temperature.", Int. J. Heat Mass Transf. 101 (2016).
[7] H. M. King, "Darcy's Law and the Field Equations of the Flow of Underground Fluids.", Trans. AIME (1956), 207: 222-239.
[8] A. Borner, et al. "High temperature permeability of fibrous materials using direct simulation Monte Carlo.", Int. J. Heat Mass Transf. 106 (2017) 1318–1326.
[9] B. K. Bessire, et al. "Decomposition of phenolic impregnated carbon ablator (PICA) as a function of temperature and heating rate." ACS applied materials & interfaces 9.25 (2017).
[10] F. Torres-Herrador, et al. "A high heating rate pyrolysis model for the Phenolic Impregnated Carbon Ablator (PICA) based on mass spectroscopy experiments." Journal of analytical and applied pyrolysis 141 (2019).
[11] B. Laub, et al. "Tutorial on Ablative TPS.", NASA Ames Research Center, Moffett Field, CA (2004).
[12] P. Ventura Diaz, et al. "High-Fidelity Simulations of HyMETS Arc-Jet Flows for PICA-N Modeling." AIAA Scitech 2021 Forum (2021).
[13] J. B.E. Meurisse, et al. "Progress Towards Modeling the Ablation Response of NuSil-Coated PICA." Ablation Workshop (2019).
[14] J. B.E. Meurisse, et al. "Multidimensional material response simulations of a full-scale tiled ablative heatshield." Aerospace Science and Technology 76 (2018).
[15] Chen, Y-K., and Frank S. Milos. "Ablation and thermal response program for spacecraft heatshield analysis." Journal of Spacecraft and Rockets 36.3 (1999).